EuroSun 2026

On the experimental characterization of the diffuse incident angle modifier: an update to ISO 9806:2025

J. M. Rodríguez-Muñoz[1] **and Fabienne Sallaberry**[2]

[1]Solar Energy Laboratory, CENUR Litoral Norte, Universidad de la República, Salto, Uruguay
[2]National Renewable Energy Centre of Spain (CENER), Sarriguren, Spain

jrodrigue@fing.edu.uy; fsallaberry@cener.com

A new version of ISO 9806 was recently adopted (ISO 9806:2025), introducing modifications to the modelling of the diffuse incident angle modifier (IAM), denoted by K_d. In the former version, ISO 9806:2017, SST derives K_d from the direct IAM assuming isotropic diffuse radiation, whereas conventional QDT fits K_d directly to experimental data. The 2025 revision adds an anisotropy correction to the SST conversion and, in QDT, permits the use of the SST diffuse-IAM treatment, in which K_d is determined from the direct IAM, alongside the conventional fitted-parameter approach. This work evaluates the effects of these modifications using test data from four collectors originally tested in accordance with ISO 9806:2017 and reprocessed under the revised procedures. The data sets cover a range of optical responses and collector technologies, including two flat-plate collectors and two heat-pipe evacuated-tube collectors, one with a compound parabolic concentrator. The results show that the 2025 modifications improve SST–QDT consistency, particularly when the SST diffuse-IAM treatment is incorporated into the QDT thermodynamic model during parameter identification. The correction has a limited effect on useful-power estimates under Blue-sky conditions; in general, it increases useful power for flat-plate collectors and slightly reduces it for evacuated-tube collectors, particularly under Hazy-sky and Gray-sky conditions and at high temperature differences.

Keywords: Incident angle modifier, diffuse solar irradiance, anisotropic effects, ISO 9806.

Field of application for the findings: test and certification.

Addressed audience: testing laboratory, researchers.

1. Introduction

Diffuse solar irradiance is an important component in the thermal performance assessment of non-concentrating solar thermal collectors, particularly under partly cloudy and overcast conditions. Its treatment is also relevant to the calculation of useful power over representative operating conditions [1]. In this context, ISO 9806 defines the thermodynamic model used to estimate useful power and specifies the steady-state testing (SST) and quasi-dynamic testing (QDT) procedures used to identify its characteristic parameters [2, 3]. In particular, the diffuse incident angle modifier (K_d, diffuse IAM) represents the optical response of a collector to the diffuse irradiance component. The diffuse component comprises sky-diffuse and ground-reflected irradiance.

In the previous version of the standard, ISO 9806:2017, SST and QDT treated the diffuse IAM differently. In SST, K_d was derived from the direct IAM, K_b, by all-sky integration under an isotropic diffuse-radiation assumption. In QDT, K_d was identified directly as a constant parameter from experimental data, thereby implicitly accounting for the anisotropic distribution of the diffuse component represented in those data. Although both methods are intended to provide equivalent collector characterizations, their different treatment of diffuse irradiance has led to systematic SST–QDT discrepancies [4, 5, 6, 7]. This is particularly relevant for collectors with tubular geometries.

In response to this problem, Rodríguez-Muñoz et al. [7] evaluated two alternative diffuse-IAM treatments within the ISO 9806:2017 framework using experimental data from a flat-plate collector (FPC) and an evacuated-tube collector (ETC). The first alternative extended to QDT the global diffuse-IAM treatment used in SST, a treatment previously proposed by Bosanac et al. outside the ISO 9806 framework [8]: K_d was calculated from K_b through all-sky integration. The second alternative separated the sky-diffuse and ground-reflected components, following the energy-calculation approach proposed by Carvalho et al. [9], and consequently required an additional solar-radiation measurement. Both alternatives improved SST–QDT consistency relative to the standard QDT fitted-parameter approach. Since their performance differences were small, the global alternative was identified as the preferred option because it combines improved consistency with simpler implementation and lower measurement requirements [7].

ISO 9806:2025 changes this situation in two related ways. It permits the SST-based calculation of K_d to be used in QDT, while retaining the conventional fitted-parameter approach, and it adds a correction intended to account for diffuse-radiation anisotropy to the all-sky integration route [3]. The global alternative previously identified as the most practical choice is therefore now included in the standard, but with an additional anisotropy correction whose effect on parameter identification, SST–QDT consistency, and useful-output estimates remains to be quantified.

This work has two objectives. First, it re-evaluates the consistency between SST and QDT in terms of both the identified characteristic parameters and the resulting useful-power estimates, considering the modifications introduced in the current version of the standard, ISO 9806:2025, related to K_d modeling. Second, it quantifies the effect of the ISO 9806:2025 anisotropy correction on useful power, including whether it increases or decreases the predicted output across collector technologies.

To address these objectives, four experimental data sets previously tested in accordance with ISO 9806:2017 are reprocessed. The data sets comprise two flat-plate collectors, one with a high-efficiency selective surface and one with a non-selective surface, and two evacuated-tube collectors with heat pipes, one of which incorporates a compound parabolic concentrator (CPC), thereby covering distinct collector technologies and optical responses. For each collector, the characteristic parameters and useful-power estimates obtained with the former and revised processing procedures are compared.

This paper is structured as follows. Section 2 describes the SST and QDT models and the diffuse-IAM procedures, with particular attention to the differences introduced by the current version of the standard, as well as the experimental data and the methodology employed for parameter identification and comparison. Section 3 presents the results, first examining the consistency between the test methods and then evaluating the impact of the anisotropy correction on useful-power calculations. Section 4 summarizes the main findings and their implications for the application of ISO 9806:2025.

2. Models, experimental data and methodology

This section presents the models, experimental data, and methodology used in the analysis. Section 2.1 describes the SST and QDT thermal-performance models and the diffuse-IAM treatments specified in ISO 9806:2017 and ISO 9806:2025. Section 2.2 presents the test facility and the four experimental data sets. Section 2.3 describes the parameter-identification procedures, and Section 2.4 defines the methodology used to compare the processing procedures and calculate useful power under standard reporting conditions.

2.1 Thermal-performance models and diffuse-IAM treatments

The ISO 9806:2017 treatment is presented first. For low-temperature glazed collectors, the quasi-dynamic testing (QDT) model established in ISO 9806 expresses useful power per unit gross area as:

$$\frac{\dot{Q}_u}{A_G} = \eta_{0,b}\left[K_b\left(\theta\right)\ G_{bt} + K_d\ G_{dt}\right] - a_1\left(\vartheta_m - \vartheta_a\right) - a_2\left(\vartheta_m - \vartheta_a\right)^2 - a_5\frac{d\vartheta_m}{dt}. \tag{1}$$

where G_{bt} and G_{dt} are the beam and diffuse irradiances in the collector plane, respectively; ϑ_m and ϑ_a are the mean fluid and ambient temperatures; and $\eta_{0,b}$, a_1, a_2, and a_5 are characteristic parameters. The direct IAM, K_b, is represented by an empirical function of the incidence angle, θ. In this work, the general IAM model is used because it can describe both uniaxial and biaxial optical responses [10]. The remaining model parameters in Eq. 1, including K_d, are identified from the experimental data.

In SST, solar irradiance is treated globally. The corresponding useful-power model is:

$$\frac{\dot{Q}_u}{A_G} = \eta_{0,hem}K_{hem}G_t - a_1\left(\vartheta_m - \vartheta_a\right) - a_2\left(\vartheta_m - \vartheta_a\right)^2 - a_5\frac{d\vartheta_m}{dt}. \tag{2}$$

The conversion from the SST parameters $\eta_{0,hem}$ and K_{hem} to the QDT parameters is specified in Annex B of ISO 9806:2017. This process is briefly described below.

First, clear-sky conditions are assumed, so that $K_{hem} = K_b$. Then, K_d is estimated from K_b by averaging it over the solid angle seen by the collector:

$$K_d^{iso} = \frac{\int_0^{\pi/2} \int_0^{\pi/2} K_b\,(\theta, \gamma) \cos(\theta) \sin(\theta) d\theta d\gamma}{\int_0^{\pi/2} \int_0^{\pi/2} \cos(\theta) \sin(\theta) d\theta d\gamma}. \tag{3}$$

The integration is evaluated by discretizing the angular domain into 10° intervals. Since the common angular increments cancel between the numerator and denominator, the discrete form is:

$$K_d^{iso} = \frac{\sum_{\theta=0^\circ}^{90^\circ} \sum_{\gamma=0^\circ}^{90^\circ} K_b\,(\theta, \gamma) \cos(\theta) \sin(\theta)}{\sum_{\theta=0^\circ}^{90^\circ} \sum_{\gamma=0^\circ}^{90^\circ} \cos(\theta) \sin(\theta)}. \tag{4}$$

The direct normal-incidence efficiency is then obtained from:

$$\eta_{0,b} = \frac{\eta_{0,hem}}{0.85 + 0.15 K_d}. \tag{5}$$

Equation 5 uses the reference clear-sky irradiance composition of 85% beam irradiance and 15% diffuse irradiance at normal incidence, where $K_b(0) = 1$. For the ISO 9806:2017 procedure, $K_d = K_d^{iso}$.

ISO 9806:2025 retains the integration in Eq. 3 and proposes an anisotropy correction based on the work of Hay and Davies [3, 11]. This procedure is described in Annex C of that version.

The following derivation is the authors' interpretation of the ISO correction; it is provided to clarify its physical meaning and is not stated explicitly in the standard.

In the general Hay–Davies formulation, the total diffuse irradiance in the collector plane, G_{dt}, is divided into an isotropic sky-background component, G_{dt}^{iso}, and a circumsolar component, G_{dt}^{cs}, associated with radiation around the solar disk. The anisotropy index $A_i = G_b/G_{sc}$ is the ratio between the beam normal irradiance, G_b, and the extraterrestrial solar irradiance, G_{sc}; it determines the fraction assigned to the circumsolar component:

$$G_{dt} = G_{dt}^{iso} + G_{dt}^{cs}, \qquad G_{dt}^{iso} = (1 - A_i) G_{dt}, \qquad G_{dt}^{cs} = A_i G_{dt}.$$

The isotropic component represents the diffuse background received from the full sky dome and is represented by the hemispherically averaged modifier K_d^{iso}. The circumsolar component is assumed to arrive from the beam direction and is therefore represented by $K_b(\theta)$. The corresponding general anisotropic diffuse modifier is:

$$K_d^{\text{ani}\prime}(\theta) = (1 - A_i) K_d^{iso} + A_i K_b(\theta).$$

In a general Hay–Davies application, A_i varies with the instantaneous beam irradiance and therefore with sky condition: it tends to zero under overcast conditions and increases in clear-sky conditions. For parameter conversion, ISO 9806:2025 imposes normal incidence, for which $K_b(0) = 1$, and the clear-sky reference values $G_b = 850$ W/m^2 and $G_{sc} = 1367$ W/m^2. Hence, $A_i = 0.622$ for this reference condition, and the general expression reduces to:

$$K_d^{ani} = K_d^{iso} \left(1 - \frac{G_b}{G_{sc}}\right) + \frac{G_b}{G_{sc}}. \tag{6}$$

Equation 6 is therefore a clear-sky, normal-incidence conversion of the parameters, rather than a time-varying application of the Hay–Davies model to each experimental record. The prime in $K_d^{\text{ani}\prime}(\theta)$ distinguishes the general, angle-dependent modifier from the ISO reference parameter K_d^{ani} defined by Eq. 6. To calculate $\eta_{0,b}$, Eq. 5 is used with $K_d = K_d^{ani}$.

Figure 1 shows the anisotropy correction at the prescribed clear-sky reference condition used in Eq. 6, that is, K_d^{ani} as a function of K_d^{iso}. In a sky-condition-dependent application, A_i would tend to zero under overcast conditions, and K_d^{ani} would consequently tend to K_d^{iso}. It is important to note that collectors can generally be grouped according to whether their diffuse IAM is lower or higher than unity. Accordingly, the figure shows that, when $K_d^{iso} < 1$, the corrected value is higher than the isotropic value, whereas, when $K_d^{iso} > 1$, the corrected value is lower.

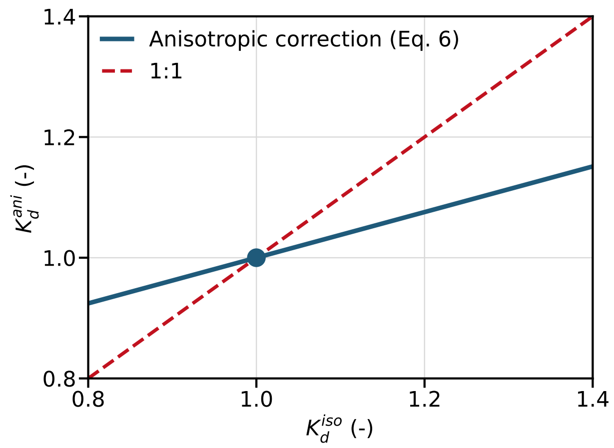

Fig. 1: Effect of the ISO 9806:2025 anisotropy correction on the diffuse IAM at the prescribed clear-sky reference condition. The red dashed line is the $K_d^{ani} = K_d^{iso}$ identity.

ISO 9806:2025 additionally permits a second QDT configuration, referred to hereafter as *QDT-new*. In this configuration, K_d^{ani} is calculated from the direct IAM through Eqs. 3 and 6 and is incorporated into the thermodynamic model. Thus, K_d is determined by K_b. The parameters defining K_b and all other free coefficients are fitted simultaneously to the experimental data. Table 1 summarizes the cases considered for each version of the standard.

Tab. 1: Diffuse-IAM treatments established in each version of the standard.

Test method	ISO 9806:2017	ISO 9806:2025
SST	K_d^{iso} (Eq. 3)	K_d^{ani} (Eq. 6)
QDT	K_d fitted	K_d fitted (unchanged)
QDT-new	not permitted	K_d^{ani} (Eq. 6)

2.2 Test facility and experimental data sets

Testing was conducted at the Solar Heater Test Bench (BECS) of the Solar Energy Laboratory (LES), Universidad de la República, in Salto, Uruguay (31.28° S, 57.92° W). A photograph of the test facility is shown in Fig. 2. The thermal-fluid circuit, measurement instrumentation, and data-acquisition system comply with the requirements of ISO 9806 for collector testing. A detailed description of the test facility and its measurement procedures is provided by Rodríguez-Muñoz et al. [12].

Fig. 2: Solar Heater Test Bench (BECS) at the Solar Energy Laboratory, Universidad de la República, Salto, Uruguay.

It is important to note that, in 2018, the test facility participated in a Latin American laboratory intercomparison organised by the Physikalisch-Technische Bundesanstalt (PTB), the German national metrology institute, with support from Solar- und Wärmetechnik Stuttgart (SWS, Germany). The exercise validated both test methods, SST and QDT, for flat-plate collectors [13]. That collector continues to be tested periodically as a quality-assurance measure to monitor the consistency of the results.

For this work, data from four collectors previously evaluated in accordance with ISO 9806:2017 were used; no new tests were introduced. The original data sets were reprocessed using the former and revised diffuse-IAM procedures with both test methods. The collectors comprise:

- **FPC-1**: flat-plate collector with a high-efficiency selective absorber surface.
- **FPC-2**: flat-plate collector with a non-selective absorber surface.
- **ETC-HP**: evacuated-tube collector with heat pipes.
- **ETC-HP-CPC**: the ETC-HP collector fitted with a compound parabolic concentrator (CPC).

2.3 Parameter identification

This section describes the procedures used to identify the characteristic parameters for each test method.

For SST, the thermal-efficiency parameters and the direct IAM were identified using the same procedures for both versions of ISO 9806, based on 10-min averages of the measured variables [2, 3]. The only difference lies in the parameter conversion: for ISO 9806:2025, the diffuse IAM used in this conversion is corrected for anisotropy, as described in Section 2.1 and Eq. 6.

For QDT parameter identification, two approaches are commonly used: multiple linear regression (MLR) and Dynamic Parameter Identification (DPI) [14]. They differ in their treatment of the transient collector response. DPI integrates the transient collector model and identifies the characteristic parameters through a non-linear least-squares adjustment. DPI was used in this work because it provides a better treatment of transient effects, particularly for evacuated-tube collectors with heat pipes, and has been shown to provide more reliable parameter estimates and useful-power predictions [15].

For all DPI configurations, the general nodal representation of the direct IAM, K_b, was used [10], with angular calculations discretized at 10° intervals. The experimental data were averaged over 30 s. Keeping the same direct-IAM representation and data-averaging interval for all configurations isolates the effect of the diffuse-IAM treatment. In QDT-new, Eqs. 3 and 6 were incorporated into the thermodynamic model and the DPI algorithm.

2.4 Methodology

The methodology was organized in two stages to address the objectives stated in the Introduction. The consistency between SST and QDT and the effect of the anisotropy correction were assessed by comparing both the identified characteristic parameters and the resulting useful-power estimates under standard reporting conditions.

In the first stage, the characteristic parameters of the four collectors were identified from the experimental data following the procedures described in Section 2.3, for all methodological cases listed in Table 1.

In the second stage, which complements the first, useful power was calculated for each parameter configuration under standard reporting conditions. Normal incidence ($K_b = 1$) and steady-state operation ($d\vartheta_m/dt = 0$) were assumed. The useful-power model therefore reduces to:

$$\frac{\dot{Q}_u}{A_G} = \eta_{0,b} \left(G_{bt} + K_d G_{dt}\right) - a_1 \left(\vartheta_m - \vartheta_a\right) - a_2 \left(\vartheta_m - \vartheta_a\right)^2 . \tag{7}$$

Four temperature differences, $\vartheta_m - \vartheta_a = 0$, 20, 40, and 60 K, were considered. The standard reporting conditions in Table 2 represent blue, hazy, and gray sky conditions. Negative calculated useful-power values were set to zero.

Tab. 2: Standard reporting conditions used for the useful-power comparison [2].

Sky condition	G_{bt} (W/m^2)	G_{dt} (W/m^2)
Blue sky	850	150
Hazy sky	440	260
Gray sky	0	400

3. Results

The following sections present the results of the two stages outlined in the previous section.

3.1 Parametric identification results

Table 3 presents the characteristic parameters obtained for each collector and for the four configurations defined in Table 1: SST-2017, SST-2025, QDT (same for both versions), and QDT-new (only for the 2025 version). For simplicity in reporting the data, the thermal capacity per unit gross area is not reported, and only selected direct-IAM nodes are included to support comparison of the optical response.

Tab. 3: Characteristic parameters and selected direct-IAM nodes for all collector data sets.

Flat-plate collectors								
Collector	FPC-1				FPC-2			
Test method	SST		QDT	QDT-new	SST		QDT	QDT-new
Standard version	2017	2025	2017–2025 (unchanged)	2025	2017	2025	2017–2025 (unchanged)	2025
$\eta_{0,b}$	0.746	0.738	0.736	0.738	0.608	0.600	0.606	0.607
K_d	0.875	0.953	0.974	0.954	0.858	0.946	0.954	0.947
a_1	4.519	4.519	4.393	4.408	4.394	4.394	4.875	4.881
a_2	0.000	0.000	0.001	0.001	0.010	0.010	0.005	0.005
$K_b(50°)$	0.940	0.940	0.938	0.938	0.929	0.929	0.915	0.916

Evacuated-tube collectors								
Collector	ETC-HP				ETC-HP-CPC			
Test method	SST		QDT	QDT-new	SST		QDT	QDT-new
Standard version	2017	2025	2017–2025 (unchanged)	2025	2017	2025	2017–2025 (unchanged)	2025
$\eta_{0,b}$	0.372	0.374	0.364	0.378	0.431	0.427	0.424	0.431
K_d	1.041	1.015	1.392	1.037	0.896	0.961	1.160	0.964
a_1	1.559	1.559	1.578	1.614	0.934	0.934	0.758	0.658
a_2	0.000	0.000	0.000	0.000	0.003	0.003	0.003	0.002
$K_{b,L}(50°)$	0.800	0.800	0.800	0.800	0.833	0.833	0.785	0.795
$K_{b,T}(20°)$	1.085	1.085	1.096	1.107	0.971	0.971	0.956	0.958
$K_{b,T}(40°)$	1.311	1.311	1.369	1.368	0.961	0.961	0.928	0.933
$K_{b,T}(60°)$	1.484	1.484	1.562	1.570	1.296	1.296	1.393	1.404

First, the results are examined from the perspective of consistency between the two test methods, with particular emphasis on the two modifications introduced in ISO 9806:2025: the anisotropy correction in SST and its incorporation into QDT-new.

Table 3 shows that, under ISO 9806:2017, the K_d values obtained by QDT are higher than those obtained by SST for all four data sets, confirming the inconsistency previously reported between the two routes [7]. The differences are moderate for the flat-plate collectors, reaching 0.099 for FPC-1 and 0.096 for FPC-2, but substantially larger for the evacuated-tube collectors: 0.351 for ETC-HP and 0.264 for ETC-HP-CPC.

For ISO 9806:2025, the SST conversion is modified through the anisotropy correction. When compared with conventional QDT, which continues to identify K_d by fitting it directly to the experimental data, the correction improves SST–QDT agreement for the flat-plate collectors, reducing the differences to 0.021 for FPC-1 and

0.008 for FPC-2, and for ETC-HP-CPC, where the difference decreases from 0.264 to 0.199. In contrast, for ETC-HP, the difference increases from 0.351 to 0.377. Thus, the anisotropy correction improves agreement with conventional QDT for collectors with some optical responses, but does not ensure consistency for all collector technologies. The resulting changes in K_d follow the mapping illustrated in Fig. 1: values with $K_d^{iso} < 1$, as for the flat-plate collectors and ETC-HP-CPC, increase after the correction, whereas values with $K_d^{iso} > 1$, as for ETC-HP, decrease; the correction leaves $K_d^{iso} = 1$ unchanged.

QDT-new incorporates the same K_d treatment used in SST into the QDT identification procedure. It substantially reduces the remaining differences with SST-2025 for all collectors: the absolute differences are 0.001 for FPC-1 and FPC-2, 0.022 for ETC-HP, and 0.003 for ETC-HP-CPC. These results show that applying this procedure in QDT provides a more robust improvement in SST–QDT consistency, as it reduces the discrepancies for all collector technologies evaluated.

Beyond K_d, only minor changes are observed in the remaining identified parameters. This behavior is consistent with the findings of Rodríguez-Muñoz et al. [7], where alternative diffuse-IAM modeling hypotheses mainly affected the diffuse terms while leaving the remaining identified parameters practically unchanged.

3.2 Useful-power comparison under standard reporting conditions

Figures 3 and 4 compare the useful-power results for the FPC-1 and ETC-HP collectors. These cases are representative of their respective collector groups and were selected to avoid overloading the figures. Each column represents one standard reporting condition, while each group of bars corresponds to one temperature difference.

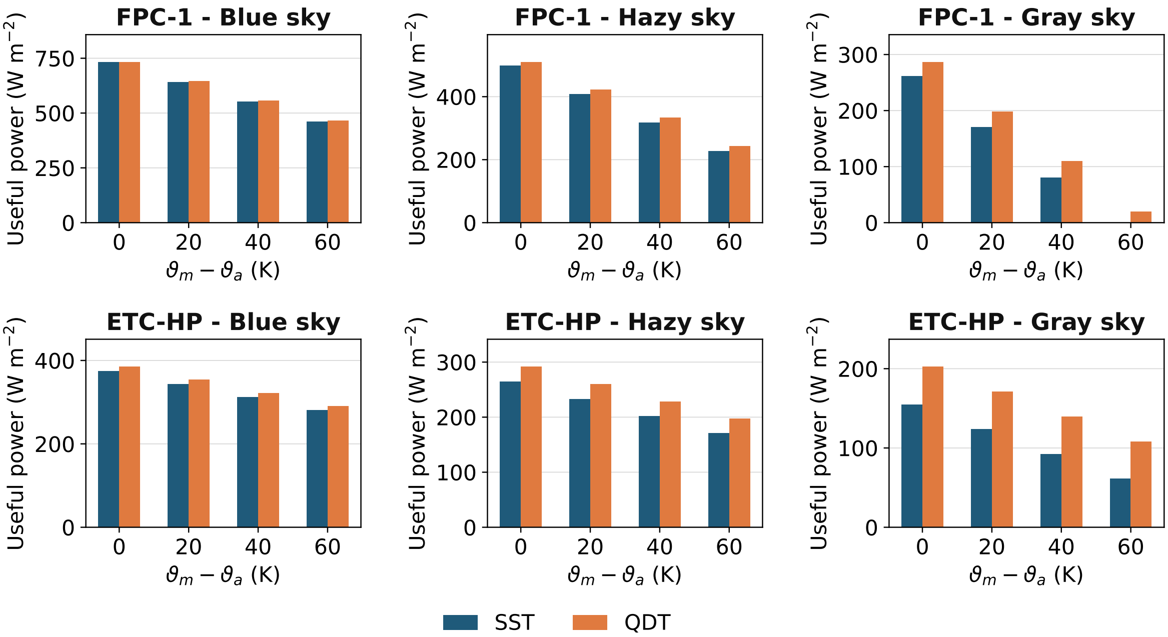

Fig. 3: Useful power predicted using SST and QDT parameter sets identified according to ISO 9806:2017. Rows correspond to FPC-1 and ETC-HP, and columns to the standard reporting sky conditions.

Figure 3 shows how the parameter discrepancy between SST and QDT under ISO 9806:2017 is translated into useful-power estimates. The differences are limited for FPC-1 but more pronounced for the evacuated-tube collectors, consistently with their larger differences in K_d. Their practical relevance depends strongly on the operating and irradiance conditions. Under Blue sky, the estimates are close because beam irradiance dominates and the thermal losses are small. The difference becomes more apparent under Hazy sky and Gray sky, where diffuse irradiance has a larger contribution, and increases further at higher temperature differences.

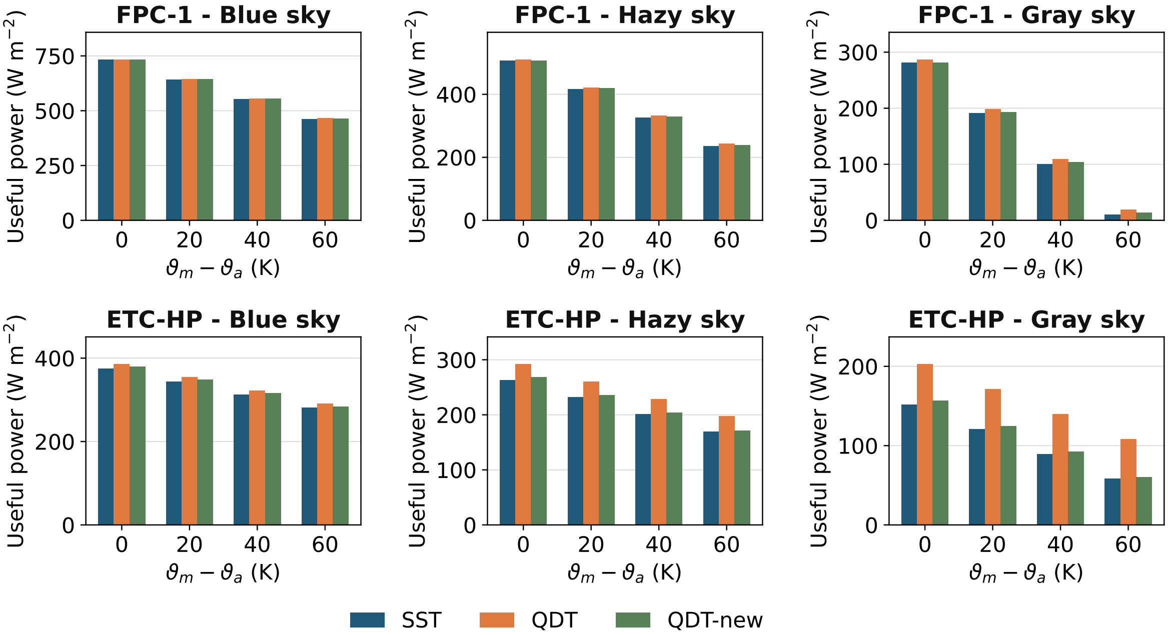

Fig. 4: Useful power predicted using SST, QDT, and QDT-new parameter sets identified according to ISO 9806:2025. Rows correspond to FPC-1 and ETC-HP, and columns to the standard reporting sky conditions.

Figure 4 confirms that the anisotropy correction generally moves the SST estimates closer to those obtained with conventional QDT. QDT-new further reinforces this agreement by applying the same anisotropy-corrected diffuse IAM during parameter identification, in line with the reconciliation of K_d values observed in Table 3. As in the 2017 comparison, the improvements are most visible under Hazy sky and Gray sky and at the highest temperature differences, whereas under Blue-sky conditions the differences between methods remain small. The useful-power results therefore confirm that the revised treatment has its greatest practical effect when diffuse-radiation contributions and thermal losses are most influential.

Beyond the improvement in SST–QDT consistency, the anisotropy correction has a direct effect on useful-power estimates. In this context, Fig. 5 directly compares the two SST conversions. For FPC-1, where $K_d^{iso} < 1$, the revised procedure increases useful power by 0.1–0.2% under Blue sky, 1.9–4.2% under Hazy sky, and 7.7–25.2% under Gray sky for temperature differences between 0 and 40 K. Conversely, for ETC-HP, where $K_d^{iso} > 1$, the correction reduces useful power by 0.1–0.2% under Blue sky, 0.4–0.6% under Hazy sky, and 2.0–5.0% under Gray sky. Thus, the effect is very small under clear-sky conditions and becomes more noticeable as the diffuse-radiation contribution increases.

The anisotropy correction accounts for the directional distribution of diffuse irradiance and is therefore expected to be more appropriate under the prescribed clear-sky reference conditions. However, Eq. 6 uses a fixed clear-sky anisotropy index, $A_i = G_b/G_{sc}$. In a sky-condition-dependent formulation, A_i would tend to zero under overcast conditions, and K_d^{ani} would consequently tend to K_d^{iso}. This behavior is not incorporated into the fixed ISO conversion and may introduce systematic deviations in useful-energy estimates for sites with a substantial frequency of cloudy conditions. A time-resolved anisotropy correction that depends on the prevailing sky conditions should therefore be evaluated to assess long-term collector performance. The discrepancy relative to the fixed ISO conversion will depend on the local distribution of sky conditions throughout the year; quantifying this effect is left for future work.

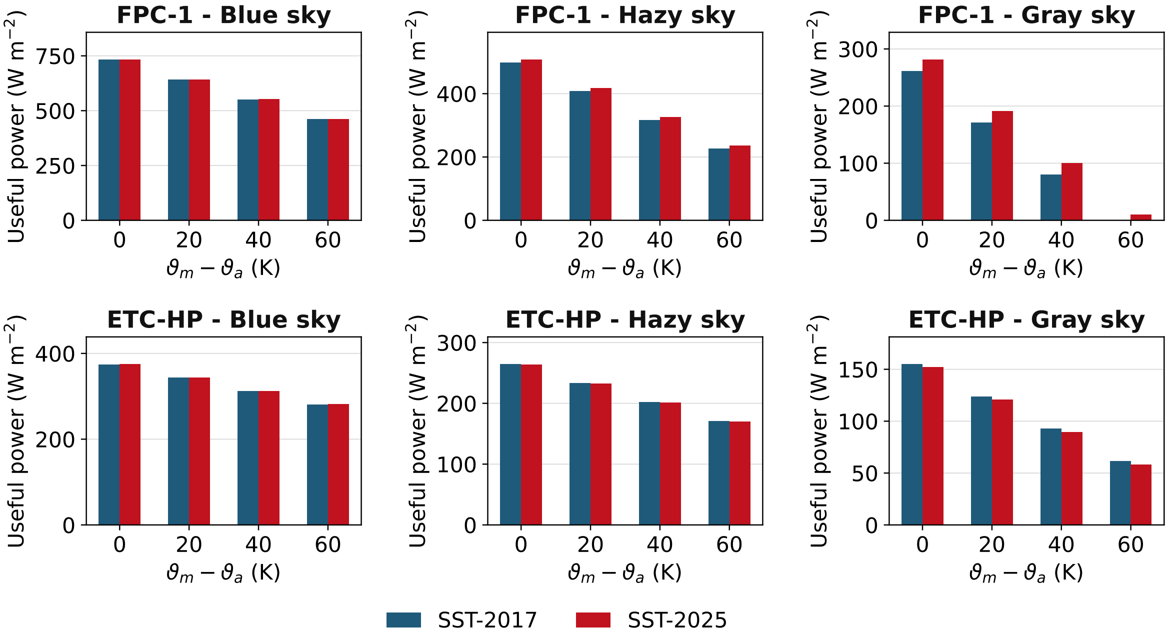

Fig. 5: Direct comparison of SST useful-power estimates obtained from the ISO 9806:2017 and ISO 9806:2025 parameter conversions. Rows correspond to FPC-1 and ETC-HP, and columns to the standard reporting sky conditions.

4. Conclusions

A new version of ISO 9806 was recently adopted (ISO 9806:2025), which introduces modifications to diffuse-IAM modelling. This work evaluates the effect of these modifications using test data from four collectors originally tested in accordance with ISO 9806:2017 and reprocessed under the revised procedures. The data sets cover a range of optical responses and collector technologies, including two flat-plate collectors and two heat-pipe evacuated-tube collectors, one of which incorporates a compound parabolic concentrator (CPC).

Under ISO 9806:2017, conventional QDT, in which K_d is fitted directly to the experimental data, produced higher K_d values than SST for all four data sets, confirming the inconsistency between the two test methods. The anisotropy correction introduced in ISO 9806:2025 improves SST–QDT agreement for the flat-plate collectors and the ETC-HP-CPC, but it does not ensure consistency for every collector technology. In addition, when the same anisotropy-corrected diffuse-IAM treatment used in SST was incorporated into the QDT thermodynamic model during parameter identification, agreement with SST-2025 improved consistently for all four collectors.

The useful-power comparison confirms that the improved consistency at the parameter level is also reflected in the predicted output. Differences between methods are most evident under Hazy-sky and Gray-sky conditions and at high temperature differences, where diffuse irradiance and thermal losses have a greater relative influence; under Blue-sky conditions, the estimates remain close.

Beyond its effect on SST–QDT consistency, the anisotropy correction has a direct effect on useful-power estimates. For collectors with $K_d^{iso} < 1$, typically flat-plate collectors and some evacuated-tube designs, it increases both K_d and useful power. Conversely, for collectors with $K_d^{iso} > 1$, a response more commonly found in evacuated-tube collectors, it decreases both quantities. The effect is very small under Blue-sky conditions and becomes more pronounced as the diffuse-radiation contribution increases.

Although the ISO 9806:2025 correction accounts for the directional distribution of diffuse irradiance, it uses a fixed anisotropy index prescribed for clear-sky conditions. A time-resolved, sky-condition-dependent formulation would tend towards the isotropic treatment under overcast conditions and should be evaluated for long-term collector-performance and useful-energy estimates. The discrepancy relative to the fixed ISO conversion will depend on the local distribution of sky conditions throughout the year; quantifying this effect is left for future work.

Acknowledgements

The authors acknowledge the financial support provided by the Comisión Sectorial de Investigación Científica (CSIC) of the Universidad de la República through its Research and Development Groups program.

References

[1] Pedro Horta, Maria João Carvalho, Manuel Collares Pereira, and Wildor Carbajal. Long-term performance calculations based on steady-state efficiency test results: Analysis of optical effects affecting beam, diffuse and reflected radiation. *Solar Energy*, 82(11):1076–1082, 2008.

[2] ISO-9806. Solar energy – solar thermal collectors – test methods. Standard, International Organization of Standarization, Switzerland, 2017.

[3] ISO-9806. Solar energy – solar thermal collectors – test methods. Standard, International Organization of Standarization, Switzerland, 2025.

[4] Peter Kovács, Ulrik Pettersson, Martin Persson, Bengt Perers, and Stephan Fischer. Improving the accuracy in performance prediction for new collector designs. In *Proceedings of Solar World Congress*, 2011.

[5] E. Zambolin and D. Del Col. An improved procedure for the experimental characterization of optical efficiency in evacuated tube solar collectors. *Renewable Energy*, 43:37–46, 2012.

[6] Tiago Osório and Maria João Carvalho. Testing of solar thermal collectors under transient conditions. *Solar Energy*, 104:71–81, 2014.

[7] J. M. Rodríguez-Muñoz, I. Bove, and R. Alonso-Suárez. Experimental characterization of the diffuse incident angle modifier of solar thermal collectors: Improving consistency between test methods. *Renewable Energy*, 256:123912, 1 2026.

[8] M. Bosanac, A. Brunotte, W. Spirkl, and R. Sizmann. The use of parameter identification for flat-plate collector testing under non-stationary conditions. *Renewable Energy*, 4(2):217–222, 1994.

[9] M. J. Carvalho, P. Horta, J. F. Mendes, M. C. Pereira, and W. M. Carbajal. Incidence angle modifiers: A general approach for energy calculations. In *Proceedings of the ISES Solar World Congress*, pages 608–612, 2007.

[10] J. M. Rodríguez-Muñoz, I. Bove, and P. Galione. General incident angle modifier model for quasi-dynamic testing of solar thermal collectors. In *Proceedings of the ISES Solar World Congress*, 2025.

[11] J. E. Hay and J. A. Davies. Calculations of the solar radiation incident on an inclined surface. In *Proceedings of the First Canadian Solar Radiation Data Workshop*, pages 59–72, Ottawa, Canada, 1980. Supply and Services Canada.

[12] J. M. Rodríguez-Muñoz, I. Bove, and R. Alonso-Suárez. Novel incident angle modifier model for quasi-dynamic testing of flat plate solar thermal collectors. *Solar Energy*, 224:112–124, 2021.

[13] Stephan Fischer. Quality infrastructure for energy efficiency and renewable energy in latin america and the caribbean, report # 95309. Report, Physikalisch-Technische Bundesanstalt (PTB), 2020.

[14] S. Fischer, W. Heidemann, H. Müller-Steinhagen, and B. Perers. Collector parameter identification—iterative methods versus multiple linear regression. In *ISES Solar World Congress*, pages 14–19. International Solar Energy Society (ISES), 2003.

[15] J. M. Rodríguez-Muñoz, I. Bove, R. Alonso-Suárez, and P. A. Galione. On the choice of the parameter identification procedure in quasi-dynamic testing of low-temperature solar collectors. *Renewable Energy*, 247:122931, 2025.